Tether Damping in Space

Xiaohua He* and J. David Powell†
Stanford University, Stanford, California

This paper analyzes the damping of a long tether connecting two spacecraft, with one spacecraft much larger than the other and the tether taut along the local vertical. In particular, it investigates the longitudinal and lateral vibration damping due to tether material properties. The tether is modeled as a visco-elastic continuum without bending stiffness. Modal frequencies and damping ratios are derived in an analytical approximation form. The results show that material damping primarily affects longitudinal motion; however, some damping of the lateral motion occurs from a weak coupling of the two modes. The damping mechanism results in decay times on the order of 1 h for longitudinal motion and 2 yr for lateral motion. The jump-rope mode has a decay time of about 1.4 times that of the lateral oscillation. The prediction of tether damping in space based on data from ground testing depends highly on the model of the damping mechanism and the scale of the ground tests. Different laws of scaling have been derived according to different damping models including structural damping, internal viscous and external viscous. Existing ground-based measurements of the TSS-1 tether are analyzed with the result that the longitudinal vibration modes will have damping ratios of no less than 1.8%.

I. Introduction

TETHER applications in space were proposed in the 1960's, although the idea can be traced back to the end of the last century. In recent years, thanks to the development of space and material technology, the concept has become a viable new option in various scientific experiments and engineering applications. The first tests of tethered spacecraft were conducted on the Gemini XI and XII missions. Since then, many applications have been proposed, such as tethered microgravity experiments, tether electric power generation, tether momentum transfer, tether propulsion, and tether kinetic isolation for instrument mounts.

The dynamic analysis and simulation of tethers using various methods and models have been ongoing for years. However, the damping properties of tethers have not been treated thoroughly. No method has been reported for using ground measurements to predict tethered system damping in flight configurations. Damping ratios of the spring-mass mode of scaled-down models in ground tests have been reported[1]; however, these data are for significantly different lengths and end masses than the space applications. For most applications, tether damping is important to keep the tethered system stable and to have a quiet environment. Although damping can be supplied by active means [e.g., tethered satellite systems (TSS)[2]], it is more desirable to provide an adequate amount of passive damping. In the Kinetic Isolation Tether Experiment (KITE),[3] the tether damping property directly affects the disturbance propagation along the tether, and thus determines the effectiveness of its isolation. Therefore, methods to determine the damping of tethers and the damping of tethered systems in space needs to be developed.

Moreover, there is a jump-rope (or "skip-rope") mode that has not been thoroughly studied, though it was observed in an orbit flight experiment 20 years ago on Gemini XI.[4] Since there is no elongation variation involved in this mode, there is no damping in the mode. Lack of damping could cause trouble in some applications and, therefore, the jump-rope mode requires careful study.

The tethered satellite systems studied in this paper consist of two spacecraft connected by a long flexible tether. One of the spacecraft, the parent, has the dominant mass of the system. The system is stabilized in orbit by the gravity gradient that aligns the tether with the local vertical in its nominal position. The mass of the tether is assumed to be substantially smaller than that of the spacecraft at either end, and the tether is modeled as a uniform continuum without bending resistance. Assuming small perturbations, the dynamics of a tethered system are considered separately as pendular librations, steady elongation, and small vibrations. The focus is on small vibrations including the longitudinal, lateral, and jump-rope modes. The partial differential equations of motion are solved using the Laplace transform, i.e., in the complex frequency domain, since natural frequencies and damping ratios are of primary interest. To have a better understanding of the relations between various parameters and to avoid long computation times, solutions are given in an approximate analytical form.

The longitudinal vibration problem was solved considering the coupling from lateral vibration that results from the orbital dynamics, although the coupling effect was found to be negligible. Different damping models are applied and compared with test data of a TSS-1 tether sample. The results lead to the conclusion that the damping model is a combination of mechanisms since no one model provides a good fit to the data. The data fitting tends to favor the combination of internal and external viscous; however, the model with structural damping yields less damping in space and is, therefore, a more conservative model to adopt. The lateral vibration problem is solved considering the longitudinal coupling effect that slightly shifts the natural frequencies and introduces a slight linear damping to the in-plane lateral modes. A nonlinear damping effect in lateral vibration due to the associated elongation rate is estimated from the energy dissipation point of view. The jump-rope mode is discussed as a special case of the superposition of two lateral vibration modes in two orthogonal planes, 90 deg out of phase. There is no material damping associated with the jump-rope mode since no change in elongation occurs. However, the orbit coupling makes the jump-rope rotation alternate periodically with planar vibration that is damped.

Theoretical analysis is presented in the next section. An example of damping ratio estimation based on ground tests is given in Sec. III and is followed by the conclusion in Sec. IV.

Received Jan. 19, 1988; revision received Sept. 15, 1988.

*Ph.D. Candidate, Aeronautics and Astronautics Department.
†Professor, Aeronautics and Astronautics Department.

II. Mathematical Models and Analysis

The analysis of this paper is based on the following assumptions:

1) Both of the spacecraft are point masses.

2) The parent spacecraft is orbiting in an unperturbed circular orbit.

3) The nominal position of the tether is aligned with the local vertical.

4) Deviations from the nominal position are small compared to tether length.

5) The tether is perfectly flexible, i.e., has no bending resistance.

6) The tether is linear elastic with material damping.

The coordinate system used originates in the unperturbed circular orbit of the parent spacecraft. The roll-axis X is in the orbital velocity direction, the yaw-axis Z is pointing down along the local vertical, and the pitch-axis Y is then defined by the right-hand rule, as is shown in Fig. 1.

According to Euler-Hill's equation[5] and linear elasticity,[7] the equations of motion of the tether can be written as

$$\mu\left(\frac{\partial^2 x}{\partial t^2} - 2n\frac{\partial u}{\partial t}\right) = \frac{\partial}{\partial z}\left(T\frac{\partial x}{\partial z}\right) \tag{1}$$

$$\mu\left(\frac{\partial^2 u}{\partial t^2} + 2n\frac{\partial x}{\partial t} - 3n^2 u\right) = 3n^2 z\mu + \frac{\partial T}{\partial z} + f \tag{2}$$

$$\mu\left(\frac{\partial^2 y}{\partial t^2} + n^2 y\right) = \frac{\partial}{\partial z}\left(T\frac{\partial y}{\partial z}\right) \tag{3}$$

$$T = EA\frac{\partial u}{\partial z} \tag{4}$$

where $x = x(z,t)$, $y = y(z,t)$, and $u = u(z,t)$ are the perturbation of the point $(0,0,z)$ in X, Y, and Z directions, respectively. T is the tension force in the tether, and f is the material damping force per unit length.

$E \equiv$ Young's modulus
$A \equiv$ cross-section area of load-bearing material
$n \equiv$ orbit rate
$\mu \equiv$ tether mass per unit length

For such a space system, the frequencies of structural vibration modes (>0.01 rad/s) are much higher than those of orbital-motion-determined modes that are known as in-plane and out-of-plane pendular libration modes with natural frequencies of $\sqrt{3}n$ and $2n$ ($n \cong 0.001$ rad/s). That is, the structural vibation is decoupled from libration modes. Therefore, the libration modes are ignored in the following structural vibration analysis, and they can be analyzed separately using a rigid tether model and then superimposed.

One end of the tether is fixed on the parent spacecraft. The other end of the tether is connected to the end mass, a satellite. The end-mass effect on the lateral vibration has been analyzed by Graziani et al.[9] By virtue of the small tether mass to satellite mass ratio, the lateral displacement at the satellite end of the tether is approximately zero, excluding the libration modes. The end-mass effect on the longitudinal vibration can be considered in the variable tension at the end. As a result, the boundary conditions for the dynamic equations of the tether can be expressed as

$$x(0.t) = y(0,t) = u(0,t) = 0 \tag{5}$$

$$x(L,t) \cong y(L,t) \cong 0 \tag{6}$$

$$EA\frac{\partial u}{\partial z}(L,t) = T(L,t) \tag{7}$$

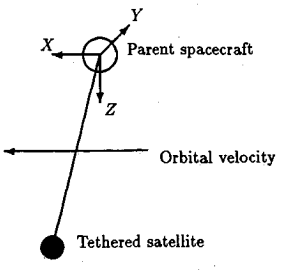

Fig. 1 Orbiting coordinate system.

Considering the dynamics of the satellite, tether tension at the end is related to the acceleration of the satellite as

$$T(L,t) = 3n^2 LM - M\frac{\partial^2 u}{\partial t^2}(L,t) = 3n^2 LM + \Delta T(L,t) \tag{8}$$

where M represents satellite mass, and L represents tether length.

Because of linearity, longitudinal displacement can be split into two parts as

$$u = u_1 + u_2 \tag{9}$$

where u_1 is the time-independent solution that represents the steady stretch due to the gravity gradient, and u_2 is the time-varying deviation of the tether displacement from u_1. By neglecting all of the time derivative terms in Eqs. (2), (4), and the boundary conditions on $u(z,t)$, a set of time-independent equations and boundary conditions for u_1 are found as

$$C_0^2\frac{\partial^2 u_1}{\partial z^2} + 3n^2 u_1 + 3n^2 z = 0 \tag{10}$$

$$u_1(0,t) = 0 \tag{11}$$

$$\frac{\partial u_1}{\partial z}(L,t) = 3n^2 ML/(EA) \tag{12}$$

where

$$C_0 = \sqrt{\frac{EA}{\mu}} \tag{13}$$

is an equivalent speed of sound in the tether. Equation (10) is solved with the solution given in Eq. (14), which is the steady elongation of the tether due to the gravity gradient.

$$u_1(z) = K_1 \sin\left(\frac{\sqrt{3}n}{C_0}z\right) - z \tag{14}$$

where

$$K_1 = \frac{1 + 3n^2 LM/(EA)}{\frac{\sqrt{3}n}{C_0}\cos\left(\frac{\sqrt{3}n}{C_0}L\right)} \tag{15}$$

Assuming a small perturbation, $|u_2| \ll |u_1|$, and according to Eqs. (9), (4), and (14), the tension force can be written as

$$T \cong EA\frac{\partial u_1}{\partial z} = EA\left[\left(1 + \frac{3n^2}{\omega_m^2}\right)\frac{\cos(\sqrt{3}nz/C_0)}{\cos(\sqrt{3}nL/C_0)} - 1\right] \tag{16}$$

where

$$\omega_m \equiv \sqrt{\frac{EA}{LM}} \tag{17}$$

Considering that $(nz/C_0) < (nL/C_0 \ll 1$, the tension can be represented by its average value along the tether:

$$T \cong EA\left[\left(\frac{\sqrt{3}n}{\omega_m}\right)^2 + \left(\frac{nL}{C_0}\right)^2\right] \tag{18}$$

With the preceding approximation, the dynamic equations of the tether can be written as

$$\frac{\partial^2 x}{\partial t^2} - (\alpha C_0)^2 \frac{\partial^2 x}{\partial z^2} - 2n\frac{\partial u_2}{\partial t} = 0 \tag{19}$$

$$\frac{\partial^2 u_2}{\partial t^2} - 3n^2 u_2 + 2n\frac{\partial x}{\partial t} = C_0^2 \frac{\partial^2 u_2}{\partial z^2} + \frac{f}{\mu} \tag{20}$$

$$\frac{\partial^2 y}{\partial t^2} + n^2 y - (\alpha C_0)^2 \frac{\partial^2 y}{\partial z^2} = 0 \tag{21}$$

with boundary conditions (5), (6), and

$$\frac{\partial u_2}{\partial z}(L,t) = \frac{1}{EA}\Delta T(L,t) \tag{22}$$

where

$$\alpha \equiv \frac{\sqrt{3}n}{\omega_m}\sqrt{1+\frac{\eta}{3}} \tag{23}$$

and

$$\eta \equiv \frac{\mu L}{M} \tag{24}$$

A. Longitudinal and In-Plane Lateral Dynamics

The longitudinal and in-plane lateral dynamics are linearly coupled through orbit rotation and are described by Eqs. (19) and (20) with boundary conditions (5), (6), and (22). According to the theory of elasticity, there are two commonly used models to describe material damping, i.e., structural damping and viscous damping. Both can be written as

$$f = bEA\frac{\partial^2}{\partial z^2}\left(\frac{\partial u_2}{\partial t}\right) \tag{25}$$

In the case of viscous damping, b is a constant damping coefficient. In the case of structural damping, $b(=\gamma/\omega)$ depends on the driving frequency ω, where γ is a constant structural damping coefficient.[7] Bergamaschi first presented an analysis of tether damping properties in 1986.[8] He used a damping model that was identical to what we refer to as viscous damping.

Since the natural frequencies and damping ratios of various modes are of primary interest, the Laplace transform is applied.[11] Then, Eqs. (19), (20), (22), (5), and (6) yield

$$\frac{\partial^2 X(z,s)}{\partial z^2} = \frac{-2ns}{\alpha^2 C_0^2}U_2(z,s) + \frac{s^2}{\alpha^2 C_0^2}X(z,s) \tag{26}$$

$$\frac{\partial^2 U_2(z,s)}{\partial z^2} = \frac{s^2 - 3n^2}{C_0^2(1+bs)}U_2(z,s) + \frac{2ns}{C_0^2(1+bs)}X(z,s) \tag{27}$$

$$U_2(0,s) = X(0,s) = X(L,s) - 0 \tag{28}$$

and

$$\frac{\partial U_2}{\partial z}(L,s) = \frac{1}{EA}T(L,s) \tag{29}$$

Solving the eigenproblem of the preceding equations, two kinds of dynamic modes are obtained with linear coupling: longitudinal modes and in-plane lateral modes. Considering $(\alpha^2|n/s|) \ll 1$, the solution can be written as

$$\omega_{2k} \cong 2k\omega_0\sqrt{1+(n/2k\omega_0)^2} \tag{30}$$

$$\xi_{2k} \cong \frac{b}{2}(2k\omega_0)/\sqrt{1+(n/2k\omega_0)^2} \tag{31}$$

for the kth longitudinal modal frequency and damping ratio, and

$$\omega_x k \cong 2k(\alpha\omega_0)\sqrt{1-(2n/2k\omega_0)^2} \tag{32}$$

$$\xi_{2k} \cong (2n/2k\omega_0)^2\frac{b}{2}(2k\alpha\omega_0)/\sqrt{1-(2n/2k\omega_0)^2} \tag{33}$$

for the kth in-plane lateral mode, where

$$\omega_0 \equiv \frac{\pi C_0}{2L} \tag{34}$$

This result shows that the effect of the cross coupling on longitudinal modes $(n/2k\omega_0)$ is negligible, since $(n/\omega_0) \ll 1(\sim 10^{-3}$, see Sec. III). The cross-coupling effect on the in-plane lateral modes is essentially a small linear damping, so that the in-plane modes are slightly damped. However, the damping ratios are extremely small, since

$$\frac{\xi_{xk}}{\xi_{2k}} \cong \alpha\left(\frac{n}{k\omega_0}\right)^2 \ll 1(\sim 10^{-6}) \tag{35}$$

Based on the preceding analysis, we can ignore the cross coupling while studying the longitudinal dynamics, and Eq. (27) can be approximated by

$$\frac{\partial^2 U_2(z,s)}{\partial z^2} - \frac{s^2}{C_0^2(1+bs)}U_2(z,s) = 0 \tag{36}$$

where the effect of gravity gradient is on the same order as that of the cross coupling and has been neglected. The solution of Eq. (36) in terms of the unknown tether dynamic tension at the satellite attachment point is

$$U_2(z,s) = \left(\frac{L}{EA}\right)\frac{\sin(\lambda z)/(\lambda L)}{\cos(\lambda L)}\Delta T(L,s) \tag{37}$$

where

$$\lambda^2 \equiv \frac{-s^2}{C_0^2(1+bs)} \tag{38}$$

Expressing the sinusoidal functions of Eq. (37) in the factored form,[12] the tension force at the satellite end of the tether can be written in terms of displacement at the same end through a transfer function, i.e.,

$$\Delta T(L,s) = KG(s)U_2(L,s) \tag{39}$$

where the transfer function is

$$G(s) = \prod_{k=1}^{\infty}\left\{\left(\frac{2k}{2k-1}\right)^2 \times \frac{\left[s^2 + b(2k-1)^2\left(\frac{\pi C_0}{2L}\right)^2 s + (2k-1)^2\left(\frac{\pi C_0}{2L}\right)^2\right]}{\left[s^2 + b(2k)^2\left(\frac{\pi C_0}{2L}\right)^2 s + (2k)^2\left(\frac{\pi C_0}{2L}\right)^2\right]}\right\} \tag{40}$$

and

$$K \equiv \frac{EA}{L} \tag{41}$$

In the case of structural damping, $b = \gamma/\omega$ is not a constant, but input-dependent, and Eq. (40) is not a conventional transfer function. However, when $(\gamma^{1.5}/2) \ll 1$, the frequency response will not be changed substantially if input frequency ω is replaced by modal frequency ω_k in each second-order factor of the formal transfer function of Eq. (40). For a second-order factor, the relative error of frequency response due to the aforementioned substitution is bounded below $\gamma^{1.5}/2$. This substitution makes Eq. (40) a conventional transfer function for the structural damping case. Therefore, the transfer function in both cases can be written as

$$G(s) = \prod_{k=1}^{\infty} \left[\left(\frac{\omega_{2k}}{\omega_{2k-1}} \right)^2 \frac{(s^2 + 2\xi_{2k-1}\omega_{2k-1}s + \omega_{2k-1}^2)}{(s^2 + 2\xi_{2k}\omega_{2k}s + \omega_{2k}^2)} \right] \quad (42)$$

where

$$\xi_k = \frac{b}{2}\omega_k \quad (43)$$

In the case of viscous damping, b is a constant, whereas in the case of structural damping, $b = \gamma/\omega k$ with γ a constant.

Figure 2 shows the pole-zero locations of the tether transfer function on a complex frequency plane for both cases. Obviously, the structural damping model results in less damped high-frequency modes compared to the viscous damping model, provided the first modes have the same damping ratio. In other words, a safer, relatively more conservative damping estimate on high-frequency structural vibration is expected from the structural damping model when no adequate data on damping ratios of the higher-order modes are available to determine which model is more accurate.

Considering the dynamics of the satellite mass, the displacement at the end of the tether can be written as

$$U_2(L,s) = -\frac{1}{Ms^2}\Delta T(L,s) \quad (44)$$

The longitudinal dynamics of the tethered satellite system can be expressed in block-diagram form, as shown in Fig. 3. The characteristic equation for the combined system (the tether and end mass) is

$$1 + \left(\frac{K}{M}\right)\frac{G(s)}{s^2} = 0 \quad (45)$$

For low-frequency dynamics, the characteristic equation is solved under the assumption that $|s| \ll \omega_0$. Through some algebra and approximation, the two lowest frequency characteristic roots of the combined system are found as

$$s_m \cong -\xi_m\omega_m \pm j\omega_m\sqrt{1-\xi_m^2} \quad (46)$$

with

$$\omega_m = \sqrt{\frac{K}{M}} = \frac{2}{\pi}\sqrt{\eta}\omega_0 \quad (47)$$

and

$$\xi_m = \frac{b}{2}\omega_m \quad (48)$$

This low-frequency dynamic mode is called the mass-spring mode, since ω_m ($= \sqrt{K/M}$) is simply the natural frequency of a mass-spring system, where the equivalent spring constant is $K = EA/L$.

The parameter b could be either a constant for viscous damping, or a variable γ/ω_m for structural damping. In the case of structural damping, all dynamic modes have the same damping ratio ($\xi_m = \gamma/2$).

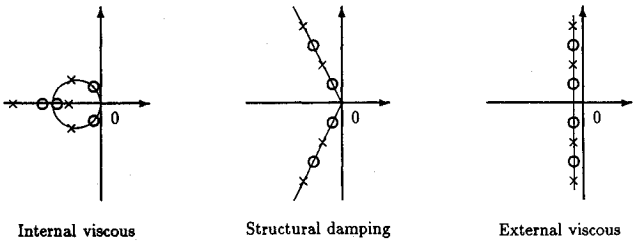

Fig. 2 Pole-zero pattern of the tether transfer function [$\Delta T(L,s)/U_2(L,s)$] with various damping models.

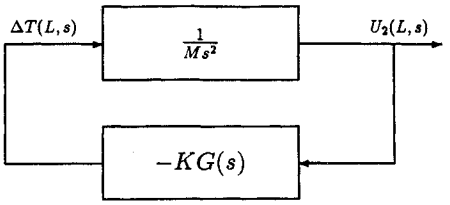

Fig. 3 Block diagram of the tether and end mass system.

The end mass (satellite) essentially affects only the mass-spring mode of the tethered system provided the tether/satellite mass ratio is small ($\eta < 1$), which will typically be the case. In the high-frequency region, the characteristic roots of tether dynamics are hardly moved as the result of the end mass effect, i.e.,

$$s_k \cong -\xi_{2k}\omega_{2k} \pm j\omega_{2k}\sqrt{1-\xi_{2k}^2} \quad (49)$$

These poles are the same as those of a tether with both ends fixed or with infinite large end masses. The deviation of poles due to the effect of finite end mass is less than $(\eta/k\pi^2)\omega_0$ for the kth mode, according to Taylor's expansion. The relative error in norm is bounded by $\eta(k\pi)^2$ that is less that 10% for most of the potential space applications. For instance, the relative error is less than 0.2% for the 2-km KITE configuration using TSS-1 tether and less than 3% for the 20-km TSS-1 configuration.

The transfer zeros of the tether/end mass combined system, shown in Fig. 3, are exactly those poles of the tether transfer function, the poles of the tether with infinite end mass. Therefore, the poles of the combined system are close to the zeros of the same system. In other words, the system zeros tend to cancel the system poles except the first low-frequency pair that are associated with the mass-spring mode. The pole-zero "cancellation" indicates that the structural vibration modes given in Eq. (49) are almost unobservable through the end mass displacement. Physically, this can be interpreted that the end point is very close to one of the node points in all the structural vibration modes, due to the small tether mass to end mass ratio, $\eta < 1$.

Another damping mechanism considered is longitudinal external viscous damping, i.e.,

$$f = b_e\mu\frac{\partial u_2}{\partial t} \quad (50)$$

The modal frequencies of all the dynamic modes are not changed by the different damping mechanism; the damping ratios are different and can be written as

$$\xi_{2k_e} = \left(\frac{b_e}{2}\right)/(2k\omega_0) \quad (51)$$

for the kth longitudinal mode, and

$$\xi_{m_e} = \left(\frac{b_e}{2}\right)\omega_m/(2\omega_0)^2 \tag{52}$$

for the mass spring mode.

B. Out-of-Plane Lateral Dynamics

Out-of-plane lateral dynamics are described in Eq. (3) with boundary conditions (5) and (6), which are decoupled from the longitudinal and the in-plane dynamics. The natural frequency of the kth out-of-plane lateral vibration mode is

$$\omega_{yk} \cong (2k\alpha\omega_0)\sqrt{1+\left(\frac{n}{2k\alpha\omega_0}\right)^2} \tag{53}$$

These modes are undamped according to linear dynamics. In practice, there will be some damping introduced by nonlinear coupling between lateral vibrations and longitudinal elongation, which also exists in the in-plane lateral vibration and will be discussed later.

The difference between the modal frequencies in the two planes is introduced by cross coupling from longitudinal motion to in-plane lateral motion and can be found by subtracting Eq. (32) from Eq. (53), i.e.,

$$\Delta\omega_k \equiv \omega_{yk} - \omega_{xk} \cong \frac{1}{2}\left(\frac{n}{2k\alpha\omega_0}\right)n \tag{54}$$

Modal frequencies in the two orthogonal planes are very close. An approximate result can be obtained from the lateral dynamic equations neglecting the cross coupling due to orbit rotation, as has been done by Suchet.[13]

Clearly, these lateral modal frequencies are much lower then those of longitudinal structural vibration modes, since $\alpha \ll 1$ for most potential tethered systems in space. It also appears that lateral vibration frequency

$$\omega_l \cong \omega_{x1} \cong \omega_{y1} \cong 2\alpha\omega_0 \cong \frac{\pi}{\sqrt{\eta}}\sqrt{3}n \tag{55}$$

is substantially greater than the orbit rate and, thus, libration frequencies ($\sqrt{3}n$, $2n$) in most cases. For the 20-km TSS-1, ω_l is 0.01 rad/s, and for the 2-km KITE tethered satellite, ω_l is 0.1 rad/s, both of which are much faster than the typical orbit rate of 0.001 rad/s. Hence, the frequency separation assumed previously is insured.

C. Nonlinear Damping in Lateral Modes

Since no bending resistance is considered, there is no (or extremely small) linear damping in the lateral (in-plane) vibration modes. However, the damping of lateral motion may be introduced by the nonlinear coupling between lateral motion and longitudinal elongation.[6] Instead of analyzing the nonlinear dynamics, the nonlinear damping effect in lateral motion is estimated from an energy point of view as a first-order approximation. If we consider the elongation engaged in the lateral deformation, an elongation rate and, thus, energy dissipation exists via the damping properties of the longitudinal motion. Since the modal frequencies of in-plane X-Z, and out-of-plane Y-Z, lateral vibration are fairly close, the following discussion of the damping property of lateral vibration applies to both cases, with modal frequencies approximated as

$$\omega_{xk} \cong \omega_{ky} \cong k\omega_l \tag{56}$$

It is reasonable to assume that the longitudinal strain engaged in lateral deformation is uniformly distributed along the tether. Then the maximum tether elongation engaged in the kth lateral vibration mode can be expressed approximately as

$$\Delta L \cong (k\pi/2)^2(B_k/L)B_k \tag{57}$$

provided the ratio of lateral vibration amplitude B_k to tether length L is small, $(B_k/L) \ll 1$.

The uniform stretch due to lateral vibration is virtually equivalent to the mass-spring mode. The energy dissipated in each cycle of the force vibration can be expressed as[7]

$$\Delta E_l = C_l\pi\omega(\Delta L)^2 \tag{58}$$

where $C_l \equiv 2\xi_m\omega_m M$, and the driving frequency is the lateral vibration modal frequency $\omega = k\omega_1 = 2k\alpha\omega_0$. On the other hand, the energy dissipated in each cycle of the kth lateral vibration mode can be written equivalently as

$$\Delta E_k = C_k\pi\omega B_k^2 \tag{59}$$

Since the energy dissipated in lateral vibration is entirely due to the associated elongation rate, the energy loss given in Eqs. (58) and (59) should be the same, i.e.,

$$\Delta E_l = \Delta E_k \tag{60}$$

Accordingly, with the equivalent damping coefficient defined by

$$C_k \equiv 2\xi_k(k\omega_l)(\mu L) \tag{61}$$

the damping ratio of the kth lateral vibration mode is

$$\xi_k = \left(\frac{1}{2\alpha}\right)\left(\frac{k\pi}{2}\right)^2(B_k/L)^2\left(\frac{b}{2}\omega_0\right) \tag{62}$$

This damping ratio is not, as is usually the case, a constant, because the damping in lateral motion is introduced by the longitudinal elongation rate through nonlinear coupling. Compared to linear damping of in-plane modes due to orbit coupling, the nonlinear damping may be either larger or smaller depending on the amplitude of the vibration, which is shown in the ratio

$$\frac{\xi_k}{\xi_{xk}} \cong k\left[\frac{B_k/L}{(4\alpha n/k\pi\omega_0)}\right]^2 \tag{63}$$

For poorly damped vibrations, amplitude-decay time may be more meaningful than the damping ratio. With Eqs. (62), (56), and (55), the decay time constant can be defined as

$$\tau_{Dk} \equiv \frac{1}{\xi_k\omega_k} \equiv \left(\frac{2}{k\pi}\right)^3 \frac{L}{\left(\frac{b}{2}\omega_0\right)C_0}/(B_k/L)^2 \tag{64}$$

Apparently, the first mode has the longest decay time. The envelope of its amplitude is governed by

$$\frac{dB_1}{dt} = -\frac{1}{\tau_{D1}}B_1 \tag{65}$$

where τ_{D1} is a function of B_1. The time required for the amplitude to decay from B_i to B_f can be found by integrating Eq. (65), and can be written as

$$\tau_1 = \frac{(2/\pi)^3 L}{2(b\omega_0/2)C_0}\left[\frac{1}{(B_f/L)^2} - \frac{1}{(B_i/L)^2}\right] \tag{66}$$

Obviously, the lateral vibration is poorly damped for small amplitudes. When the lateral vibration amplitude is 1% of tether length, it will take weeks or months for 90% amplitude decay, even if the longitudinal vibration of the tether were critically damped $\{[(b/2)\omega_0] = 1\}$. Additional damping devices, possibly active, may be required for the applications demanding low dynamic noise and high stability.

D. Jump-Rope Mode

The jump-rope mode is a rigid-body revolution of the tether between its two ends. Basically, it consists of the lateral mode shapes rotating about an axis along the nominal tether position, similar to the motion of a rope when a person is playing jump-rope or skip-rope. The jump-rope mode was first observed in space during the Gemini XI mission. It was excited near the termination of tether deployment and subsided later due to tether slack.[4] The jump-rope mode can be explained by prior lateral motion analysis in this paper. It is actually a special case involving the superposition of the in-plane and out-of-plane lateral vibration modes. In this special case, vibrations in both planes have the same frequency and amplitude, but differ in phase by 90 deg.

In a pure jump-rope mode, the dynamics have no damping, since there is no elongation change, although a constant elongation exists. However, for a tether stretched vertically in orbit, there are two effects of orbital coupling that would destroy or prevent pure jump-rope mode. One of the effects is the slight linear damping in the in-plane lateral modes. The other effect is the frequency difference between lateral modes in the two orthogonal planes.

The effect of linear damping in the in-plane motion on a jump-rope mode is to attenuate any motion in the orbit plane, so that the rotation would eventually become a planar vibration in the plane orthogonal to the orbit plane. However, the time for the in-plane motion to die out may be extremely long, practically forever. The exponential decay of the in-plane motion has a time constant of

$$\tau_J = \frac{1}{\xi_{xk}\omega_{xk}} = \frac{1}{4\pi\alpha^2 nb}\left(\frac{2\pi}{n}\right) \tag{67}$$

which may be in the order of 10^8 orbit periods.

The frequencies of lateral vibration modes in two planes are different by $\Delta\omega_k$ for the kth mode, as is given in Eq. (54). This frequency difference kills a pure jump-rope rotation by changing the phase difference of the vibration modes in two orthogonal planes. An exchange occurs between jump-rope rotation and planar lateral vibration, thus producing a beat phenomenon. As discussed earlier, planar lateral motion introduces an elongation rate and material damping. The beat frequency is one-half of the frequency difference given in Eq. (54). In each cycle of the beat, the mode of motion alternates twice between pure rotation and planar vibration. Figure 4 illustrates the end view of mode shapes of the beating jump-rope motion in different moments. For the kth mode, the beat time period is

$$\tau_{Jk} = \frac{\pi}{\Delta\omega_k} = \left(\frac{2k\alpha\omega_0}{n}\right)\left(\frac{2\pi}{n}\right) \tag{68}$$

where $(2\pi/n)$ is the orbital period.

Intuitively, the lowest energy mode, the first mode, is the one most easily excited. Equation (68) shows that it has the shortest beat period. In other words, it will first become a pure planar vibration in $\tau_1/4$ (5 orbit periods for the case of a 20-km TSS-1 tether, and 22 orbit periods for the case of a 2-km TSS-1 tether) after being excited, and will come back to pure jump-rope rotation in another $\tau_1/4$ with decreased amplitude. The beating jump-rope mode is poorly damped, since lateral planar vibration, where the damping originates, is also poorly damped. The amplitude of the curve made of the jumping "rope" can be expressed as

$$A_k = B_{Jk}\sqrt{\cos^2(k\omega_l t) + \cos^2(k\omega_l + \Delta\omega_k)t} = B_{Jk}\sqrt{1 + \cos(\Delta\omega_k t)\,\cos(2k\omega_l + \Delta\omega_k)t} \tag{69}$$

which indicates a beat vibration with vibration frequency of $(2k\omega_l + \Delta\omega_k)$ and beat frequency of $\Delta\omega_k$. In this mode, longitudinal stretching is varying. The same longitudinal stretching

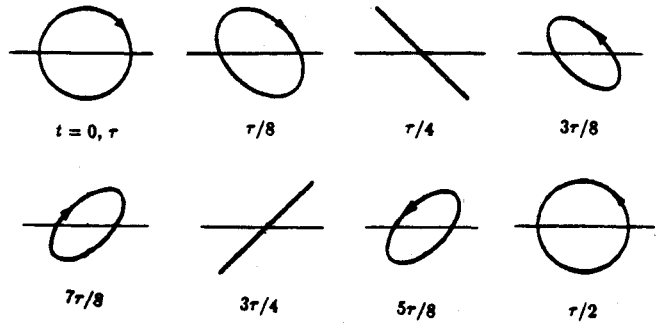

Fig. 4 End view of the "beat" mode shapes at various times.

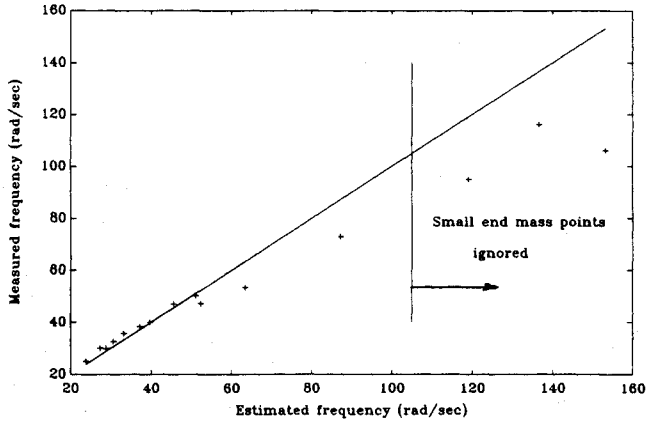

Fig. 5 Measured frequency vs estimation of linear model.

variation can also be caused by a planar vibration, which is the equivalent planar vibration associated with the beating mode. The amplitude of this equivalent planar vibration can be calculated as

$$B_k = |\Delta A_k| = B_{Jk}\left|\sqrt{1+\cos(\Delta\omega_k t)} - \sqrt{1-\cos(\Delta\omega_k t)}\right| \tag{70}$$

i.e.,

$$B_k^2 = 2[1 - |\sin(\Delta\omega_k t)|]B_{Jk}^2 \tag{71}$$

with the mean value of

$$\overline{B_k^2} = (2 - 4/\pi)B_{Jk}^2 \cong 0.73B_{Jk}^2 \tag{72}$$

Since the equivalent damping ratio due to the associated stretch is proportional to the squared amplitude of the planar vibration, the equivalent damping ratio of the beating mode is 73% of that of the corresponding planar lateral vibration mode, and thus the decay time is 1.4 times.

III. Damping Ratio and Test Data

Some experimental measurements of a tether fabricated for the TSS-1 mission have been provided by Martin Marietta Denver Aerospace, Inc.[1] The experiment was performed in a warehouse-like ambient condition. A tether sample of various lengths was hung with a load of various masses at the bottom end. After longitudinal oscillation was started by a well-controlled initial condition that excites only the mass-spring oscillation mode, the natural frequency ω_n was calculated from the output of an accelerometer mounted on the load mass. The damping ratio was also calculated from the output of the accelerometer according to a second-order system model in which the displacement of the load mass is given by

$$y(t) = Y_0 \exp(-\xi\omega_n t)\cos(\omega_n t + \phi) \tag{73}$$

The test was conducted under two different conditions, namely, preloaded and unpreloaded, i.e., with or without having the tether stretched by a large load mass hanging at the bottom for a certain time before measurement. The preloaded tethers seem to behave more linearly compared to the unpreloaded ones. In the following analysis, the preloaded measurements will be used. Examining the measured oscillation frequency, we found that it follows Eq. (47) fairly well except for a few points at the high-frequency range as can be seen in Fig. 5, especially the 3 out of 15 measurements with a small end mass (0.226 kg). This observation suggests that the configuration of the test can be modeled linearly according to the prior analysis with zero orbit rate ($\eta = 0$). We suspect that the deviations of the three measurements with small end mass might be caused by some nonlinear behavior such as recoil, creep, and creep recovery effect,[16] since the end mass was not heavy enough to pull the tether straight. Therefore, the data measured with the small end mass were considered unreliable and are left out of the following analysis.

According to the linear model derived, tether stiffness is estimated as the mean value

$$EA = \frac{1}{12}\sum_{i=1}^{12}(\omega_m LM)_i = 5.68 \times 10^4 \text{ N} \tag{74}$$

Considering the tether density[15]

$$\mu = 8.2 \text{ kg/km} \tag{75}$$

the speed of sound in the tether is

$$C_0 = \sqrt{EA/\mu} = 2632 \text{ (m/s)} \tag{76}$$

Unlike the modal frequency, the damping ratio does not have an accepted model. So far, the mechanism is not well understood for the material damping of the tether with a multilayer structure as shown in Fig. 6. Therefore, to choose or develop a model for the damping ratio is not a trivial issue. Considering the test environment, there may exist some damping due to air-friction on the tether skin and aerodynamic drag on the end mass. Fortunately, in the measured damping ratios, the components caused by the two aerodynamic effects are less than 1% according to a conservative aerodynamic analysis,[17] which suggests that the aerodynamic effects are negligible, and the measured damping is essentially cause by tether material damping.

Figure 7 shows a definite trend of measured damping ratio vs end mass. Since the structural damping model results in a damping ratio that is constant and independent of end mass, the mass-dependent trend in the measured damping ratios suggests that the structural damping model alone does not explain the test data. Figure 8 indicates that the linear proportionality to $1/\sqrt{M}$ seems to best explain the data, although a substantial scatter still exists. Figure 9 shows a nonmonotonic trend of $\xi\sqrt{M}$ vs L, which suggests a model in the form of

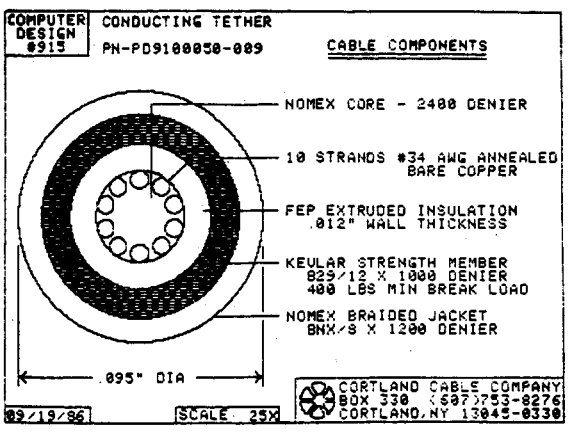

Fig. 6 Cross section of the TSS-1 tether, by Cortland Cable Company.

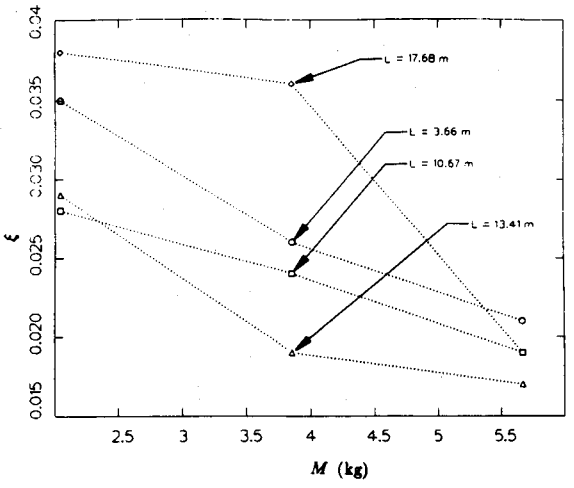

Fig. 7 Damping ratio vs end mass.

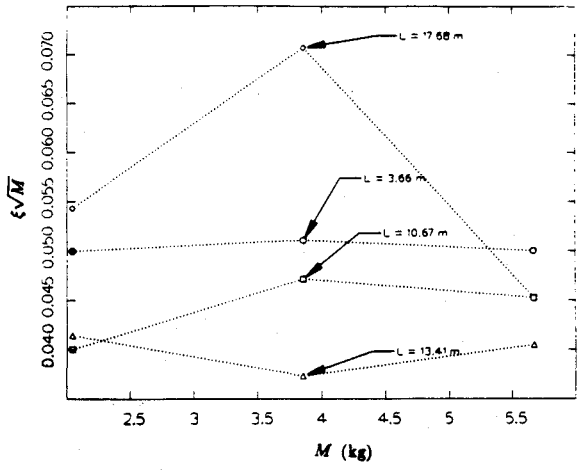

Fig. 8 Normalized (by $M^{-1/2}$) damping ratio vs end mass.

$$\xi = (a_1 L^{-\beta_1} + a_2 L^{\beta_2}) M^{-1/2} \tag{77}$$

where

$$\beta_1, \beta_2 > 0$$

Among the models discussed, the first term suggests the internal damping with $\beta_1 = 1/2$. The second term suggests the external viscous damping with $\beta_2 = 3/2$ as given in Eq. (52) with

$$b_e = \left(\frac{\pi^2\sqrt{EA}}{2\mu} a_2\right) \tag{78}$$

Considering that structural damping may also exist as a component, the general form of the damping ratio can be written as

$$\xi = (a_1 L^{-1/2} + a_2 L^{3/2}) M^{-1/2} + \gamma/2 \tag{79}$$

For comparison, we rewrite Eq. (25) as

$$f = (bEA)\frac{\partial^2}{\partial z^2}\left(\frac{\partial u_2}{\partial t}\right) = \left(\frac{2}{\sqrt{EA}} a_1\right)\frac{\partial^2}{\partial z^2}\left(\frac{\partial u_2}{\partial t}\right) \tag{80}$$

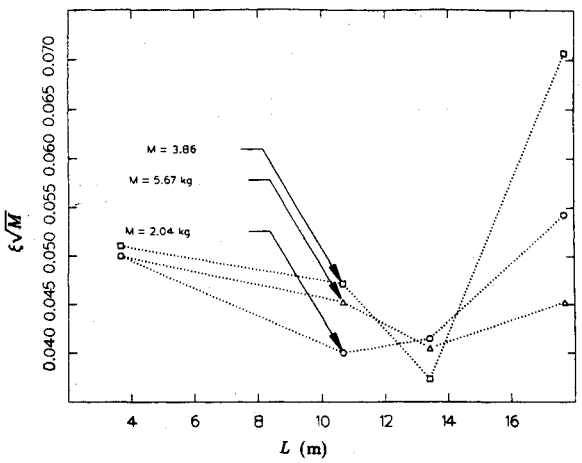

Fig. 9 Normalized (by $M^{-1/2}$) damping ratio vs tether length.

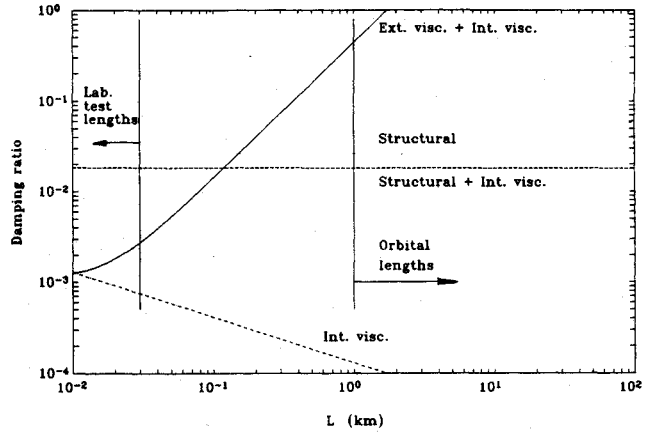

Fig. 10 Extrapolated damping ratio of long tether with 1000-kg end mass.

Table 1 Result of least-squares estimation

Model	Formula	RMS relative error
Internal viscous	$\xi = 0.13M^{-1/2}L^{-1/2}$	30%
Structural	$\xi = 0.026$	29%
Internal viscous + structural	$\xi = 0.042M^{-1/2}L^{-1/2} + 0.018$	23%
Internal + external viscous	$\xi = (0.082L^{-1/2} + 4.4\times 10^{-4}L^{3/2})M^{-1/2}$	13%

for internal viscous damping force, and

$$f = (bEA)\frac{\partial^2}{\partial z^2}\left(\frac{\partial u_2}{\partial t}\right) \cong (\sqrt{EALM}\gamma)\frac{\partial^2}{\partial z^2}\left(\frac{\partial u_2}{\partial t}\right) \qquad (81)$$

for structural damping force in the mass-spring mode.

The result of possible least-square fits with positive coefficients is given in Table 1. We noticed that the external viscous damping has the same form as the air-skin friction; but the value estimated from the test is four orders of magnitude higher than that calculated, suggesting that the external viscous damping present is not caused by air friction on the tether skin. This external damping may be explained by the friction between the internal load-bearing component and the outer coating layer of the tether, although neither the exact mechanism nor whether the mechanism would be present with orbital tether lengths is clear.

Figure 10 shows the damping ratio vs length of a tethered system wtih 1000-kg end mass, which is extrapolated from the estimated damping parameters. Different models give substantially different results for orbital lengths. Because of the small amount of test data and the fact that it was obtained with much smaller end mass (2–6 kg), it is difficult to conclude which model is more accurate. To precisely predict the damping property of a tethered system in space, further study on material damping mechanisms of tethers and more test data are necessary. However, our results show that the damping ratio would most likely be bounded between the predictions made by the two models, external viscous $a_2L^{3/2}M^{-1/2}$ as the upper bound, and structural $\gamma/2$ as the lower bound for long tethered systems. The lower bound given by tether structural damping is the same ($\gamma/2$) for all the longitudinal modes. For instance, if the TSS-1 tether is to be used, the damping ratio of all the longitudinal modes, including the mass-spring model, of a tethered satellite system will be no less than 1.8%. For a typical tethered satellite system, this damping ratio corresponds to a decay time constant of 12 min, which means an hour for 99% amplitude decay. The 1.8% damping ratio is about four times the value for a Kevlar beam tested in a vacuum chamber.[18] Compounded multilayer coating may be the main factor that causes the increase of damping. Temperature and heat transfer into air may also affect tether damping, although they are not analyzed here.

The lateral modes will be poorly damped, especially for small-amplitude vibration, because the damping ratio of the lateral mode is essentially zero no matter how large the damping ratio of the longitudinal mode is. For the case of TSS-1, according to Eq. (66), it will take 20.8 months for the lateral amplitude (normalized by tether length) to decay from an initial value of 1% to 0.1%. Choosing high-damping materials will have little effect on lateral damping.

IV. Conclusions

The damped behavior of a tethered satellite system has been analyzed with a continuum tether modeled without bending stiffness. Modal frequencies and damping ratios in terms of tether material parameters are presented in an approximate analytical form.

The dynamic model includes the damping due to a longitudinal dynamic motion, and has resulted in the determination of the role of material damping properties on the tethered system. The effect of damping was evaluated at tether lengths typical of laboratory tests and orbital lengths. The appropriate scaling relations based on different damping mechanisms were developed and their importance was demonstrated in the extrapolation of lab test data to the orbital case.

The lateral analysis included a jump-rope mode, a combination of vibrations in two orthogonal planes that are 90 deg out of phase. A damping mechanism based on the longitudinal stretching induced by lateral motion was shown to produce very long decay times. It is shown that the jump-rope rotation will alternate with planar vibration. With the small damping mechanism in the planar vibration, the decay times of the alternating modes are 1.4 times those of pure planar vibration.

Test data of a TSS-1 tether were analyzed as an example. A damping model consisting of internal viscous, external viscous, and structural damping mechanicsms have been used to fit the data. The combination of external and internal viscous damping model yields the best fit to the data, whereas the combination of structural and internal viscous damping mechanism yields a more conservative estimate of 1.8% for the damping ratio. The extrapolation of test data shows that it

takes an hour for the longitudinal oscillation to decay from initial amplitude to 1% (99% decay), but it takes about 1.7 years for the lateral vibration to decay from 1–0.1% of its length (90% decay). These results are based on test data from tether lengths of up to 30 m in the thermal and atmospheric environment of an Earth-based laboratory. Further testing in the laboratory and in the orbital environment is certainly warranted and desirable in order to establish the validity of these scaling laws and numerical results.

Possibilities for the improvement in system damping include the use of large-diameter tethers braided with different materials or devices placed at various locations along the tether. Other alternatives are active damping systems such as reel control, attachment point motion, or the use of electrodynamic forces in conductive tethers.

Acknowledgment

Research supported by NASA Ames Research Center under Grants NCC 2-389 and NCA 2-54.

References

[1]Marshall, L., Internal Memorandum TSS-86-LM-376, Martin Marietta, Denver, CO, Aug. 1986.

[2]Baracat, W. A. and Butner, C. L., *Tethers in Space Handbook*, prepared for NASA Office of Space Flight Advanced Programs, Bantam, Aug. 1986.

[3]Lemke, G., Powell, J. D., and He, X., "Attitude Control of Tethered Spacecraft," *The Journal of Astronautical Science*, Vol. 35, No. 1, Jan.–March 1987, pp. 41–56.

[4]Lang, D. D. and Nolting, R. K., "Operations with Tethered Space Vehicles," *Gemini Summary Conference,* Houston, TX, NASA SP-138, Feb. 1967.

[5]Kaplan, M. H., *Modern Spacecraft Dynamics and Control*, Wiley, New York, 1976, Chap. 3.

[6]Carroll, J. A., "Lateral Tether Damping," private communication, Aug. 1986.

[7]Meirovitch, L., *Analytical Methods in Vibrations*, Macmillan Co., London, 1967, Chaps. 5, 9.

[8]Bergamaschi, S. and Lazzarin, W., "Dynamical Effects of Tether Structural Damping: A Preliminary Model," *Proceedings of the NASA/AIAA/PSN International Conference on Tethers in Space*, Univelt, San Diego, CA, 1986, pp. 245–256.

[9]Graziani, F., Sgubini, S., and Agneni, A., "Disturbance Propagation in Orbiting Tethers," *Proceedings of the NASA/AIAA/PSN International Conference on Tethers in Space*, Univelt, San Diego, CA, 1986, pp. 301–316.

[10]Bergamaschi, S. and Cusinato, S., "Continuous Model for Tether Elastic Vibration in TSS," AIAA 24th Aerospace Sciences Meeting, Reno, NV, Jan. 1986.

[11]Bryson, A. E., "Control of Spacecraft and Aircraft," Lecture Notes, Stanford Univ., Stanford, CA, draft of Sept. 1985.

[12]Zucker, R., "Elementary Transcendental Functions Logarithmic, Exponential, Circular and Hyperbolic Functions," *Handbook of Mathematical Functions*, edited by Milton Abramowitz and Irene A. Stegun, Dover, New York, 1964, p. 75.

[13]Suchet, D., "Lateral Dynamics of a Tether," report, Dept. of Aeronautics and Astronautics, Stanford Univ., Stanford, CA, June 1986.

[14]He, X., "Attitude Control of Tethered Satellites," Ph.D. Dissertation, Stanford Univ., Aeronautics and Astronautics Dept., Stanford, CA (to be published).

[15]Scala, E. and Bentley, D. P., "Design and Fabrication of the 20 KM/10 KV Electromechanical Tether for TSS-1 Using High Impact Conductor (Hiwire)^{TM}," *Proceedings of the NASA/AIAA/PSN International Conference on Tethers in Space*, Univelt, San Diego, CA, 1986, pp. 725–731.

[16]Carroll, J. A., "Status Update on SEDS (Small Expendable Deployment system)," *Joint Review Meeting of Parallel PSN/CNR-NASA Tether Applications Studies*, General Research Corp. McLean, VA., July 1986.

[17]Hoerner, S. F., *Fluid-Dynamic Drag,* published by author, 1965, Library of Congress Catalog Card Number 64-19666.

[18]Edberg, D. L., "Measurement of Material Damping in a Simulated Space Environment," Ph.D. Dissertation, Dept. of Aeronautics and Astronautics, Stanford Univ., Stanford, CA, Dec. 1984.